

Electronic polarization in pentacene crystals and thin films

E.V. Tsiper¹ and Z.G. Soos²

¹*Department of Chemistry, Rutgers University, 610 Taylor Rd., Piscataway, NJ 08854*

²*Department of Chemistry, Princeton University, Princeton, NJ 08544*

Electronic polarization is evaluated in pentacene crystals and in thin films on a metallic substrate using a self-consistent method for computing charge redistribution in non-overlapping molecules. The optical dielectric constant and its principal axes are reported for a neutral crystal. The polarization energies P_+ and P_- of a cation and anion at infinite separation are found for both molecules in the crystal's unit cell in the bulk, at the surface, and at the organic-metal interface of a film of N molecular layers. We find that a single pentacene layer with herring-bone packing provides a screening environment approaching the bulk. The polarization contribution to the transport gap $P = P_+ + P_-$, which is 2.01 eV in the bulk, decreases and increases by only $\sim 10\%$ at surfaces and interfaces, respectively. We also compute the polarization energy of charge-transfer (CT) states with fixed separation between anion and cation, and compare to electroabsorption data and to sub-molecular calculations. Electronic polarization of ~ 1 eV per charge has a major role for transport in organic molecular systems with limited overlap.

PACS: 77.22.-d, 71.70.Ch, 71.20.Rv

I. INTRODUCTION

Prospective molecular electronic devices are based on organic films deposited on metal or semiconductor surfaces [1–3]. Due to limited mobility, organic devices are typically restricted to thin (10–100 nm) films. Variations in electronic polarization energies of charge carriers near surfaces and interfaces affect the transport states [4] and hence device function. We have recently addressed electronic polarization at surfaces and in thin films [5] using a self-consistent approach in the limit of vanishing intermolecular overlap [6], when each molecule experiences the non-uniform electrostatic potential of all other molecules. For the prototypical hole conductor [3], perylenetetracarboxylic acid dianhydride (PTCDA), the calculated transport gap varies by 500 meV between monolayers and thick films, in agreement with photoelectron and tunneling electron spectroscopy [5]. PTCDA showed that electronic polarization is accessible to self-consistent computation in crystalline thin films.

In contrast to PTCDA, whose molecules form one-dimensional stacks and lie almost flat on metallic substrates, many organic molecular crystals of interest have a herring-bone packing, with molecules oriented across molecular layers as sketched in Fig. 1. Both thiophenes [1] and acenes [2] have herring-bone packing and are suitable for thin film transistors. The molecules in crystalline thin films are almost upright and charge transport is preferentially parallel to the surface.

In this paper, we analyze electronic polarization in pentacene, considering it as a representative of a wider class of organic materials with electronic applications. We calculate electronic polarization in the bulk to obtain the optical dielectric constant, the transport gap for generating an electron-hole pair at infinite separation, and the

electrostatic binding between molecular ions at fixed separation in the lattice. We then consider the experimental situation in Fig. 1 of thin films on a metallic substrate to compute electronic polarization at the surface and at the organic-metal interface, assuming idealized films with structure identical to the bulk. Crystalline thin films exhibit multiple phases that, except in monolayers, are close to the bulk.

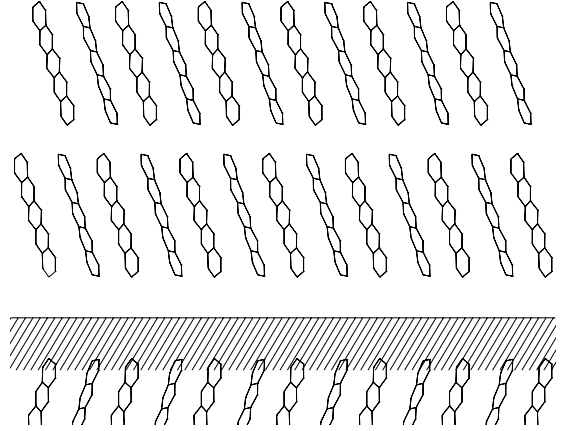


Fig. 1 Schematic molecular packing in a pentacene layer on metal. Image charges below the metal surface are also sketched.

The long axis of pentacene or α -sexithiophene is almost normal to the surface. Image charges across the interface in Fig. 1 then act in the direction of greatest polarizability, which results in contrasting electronic polarization in pentacene and PTCDA films. Electric fields normal to the surface induce large dipoles in pentacenes, but these induced dipoles are parallel and hence repulsive. There is competition between charge redistribution due to image charges and induced dipoles. Our self-consistent calculations of charge redistribution indicate that even a single molecular layer provides a screening environment that reduces repulsion between induced dipoles. The improved

iterative procedures of Section II are necessitated by the competition between image charges and induced dipoles.

The paper is organized as follows. In Section II we consider the system of linear equations for electronic polarization and introduce alternative methods based on a minimum principle when the efficient iteration scheme of [6] fails. Section III contains results for bulk crystals, including the optical dielectric constants, polarization energies of cations and anions, and the binding energies of ion pairs. In Section IV we consider pentacene films of 1–10 molecular layers and report polarization energies at the surface and at the metal-organic interface. The self-consistent pentacene potential at the surface illustrates the competition between image charges and induced dipoles. Section V contains discussion and conclusions.

II. SOLUTION OF LINEAR EQUATIONS

The zero-overlap approximation reduces electronic polarization to charge redistribution on molecules in the electrostatic potential of the solid. The crystal structure fixes all distances. We neglect lattice relaxation whose polarization is estimated to be an order of magnitude smaller in organic molecular crystals [7,8]. The crystal potential at atoms is readily introduced as site energies in semiempirical theory, which then provides a practical approach to computing self-consistent atomic charges and induced dipoles [6]. We have eight linear equations per atom and need large (10^3) clusters of molecules for long-range Coulomb interactions. The large number of equations precludes the use of algorithms based on transformations of dense matrices. For example, a cluster of 2000 PTCDA molecules, as in [6], leads to 608,000 linear equations for 38 partial atomic charges and 3×38 components of induced atomic dipoles for each atom of each molecule, and the same number of potentials and potential gradients.

We review briefly some approaches for solving linear equations that appear in polarization problems. We first recast these equations in a formal but transparent form. Let q be the vector describing charge redistribution in a cluster of interest. Its components may include partial atomic charges for each atom of each molecule, as well as induced atomic dipoles. Higher atomic multipoles can be included in q as well. Let $\rho^{(0)}$ be the “unrelaxed” charge distribution, that is the charge distribution in the individual molecules in the gas phase, the actual charge distribution thus being $\rho^{(0)} + q$.

For zero overlap, charge conservation for individual molecules leads to simple constraints on the components of q , meaning that q belongs to a certain subspace \mathcal{Q} of interest. We note that $\rho^{(0)}$ does not necessarily belong to \mathcal{Q} since the source charges on ions do not sum to zero.

The polarization problem is defined in terms of the “state vector” q as minimization of the total energy $E(q)$, which can be formally written as

$$E = \frac{1}{2}(qGq) + \frac{1}{2}(\rho^{(0)} + q|V|\rho^{(0)} + q). \quad (1)$$

We use bra- and ket- notation to denote matrix vector products. The first term is the energy of non-interacting molecules. A symmetric positive-definite *stiffness matrix* G ensures that $q = 0$ in the absence of interactions. It results from solving Schrödinger’s equation for a single molecule in non-uniform external field. The stiffness matrix is block-diagonal, with separate blocks corresponding to individual molecules or ions.

The second term describes intermolecular interactions. The interaction matrix V contains charge-charge, charge-dipole, and dipole-dipole interactions, and can also be made symmetric. The matrix V is indefinite, reflecting that Coulomb systems are always unstable. In contrast to the stiffness matrix, the diagonal blocks of V are zero, since no molecule interacts with itself.

Expression (1) shows a potential for instability, since it may have no minimum when V is sufficiently large. In the organic molecular crystals that we consider, V is small enough and only results in a shift of the minimum of $E(q)$ from $q = 0$.

Differentiating (1) with respect to q we find a set of linear equations on q :

$$Gq + Vq = -V\rho^{(0)}, \quad (2)$$

subject to the constraint that q belongs to \mathcal{Q} . While this form of polarization equations is simple conceptually, another form is often more practical. By introducing a set of *generalized potentials* $p = -Gq$ we recast (1) in a dual form:

$$p = V(\rho^{(0)} + q) \quad (3a)$$

$$q = -\Pi p, \quad (3b)$$

where $\Pi = G^{-1}$. These are formally written Eqs. (8) and (15) of [6]. The physical meaning of Eq. (3) is simple. Instead of a one-step minimization of $E(q)$ as in (2), we optimize the charge distribution of each molecule individually in the self-consistent external field p of all other molecules.

The components of the vector p contain potentials and potential gradients (and possibly higher derivatives), that couple to atomic partial charges, atomic induced dipoles, and higher atomic multipoles. The symmetric positive-definite *polarization matrix* Π has the same block-diagonal structure as G and describes the polarization response of individual molecules to the external field, given by the components of p . The inverse of G is well defined in the subspace of interest \mathcal{Q} .

A. Iterative solution of polarization equations

The dual form of Eqs. (3) suggests a natural iterative approach. We start with the bare charge distribution $\rho^{(0)}$ and find “bare” potentials $p^{(0)} = V\rho^{(0)}$. We then repeat updating charge distribution using Eq. (3b) and recalculating p using Eq. (3a) until convergence.

When convergent, this procedure is usually fast. However, it is often unstable, leading to oscillatory behavior. A simple numerical trick has been proven very powerful in suppressing such oscillations. We introduce a damping factor $0 < f < 1$ and iterate, starting with $q^{(0)} = 0$:

$$p^{(m)} = V(\rho^{(0)} + q^{(m)}) \quad (4a)$$

$$q^{(m+1)} = fq^{(m)} - (1-f)\Pi p^{(m)} \quad (4b)$$

We increase f adaptively when oscillations in $E(q^{(m)})$ are detected and decrease it when convergence is stable. All results in Refs. [6,5,9] were obtained using this iteration procedure, which appears to be both remarkably stable and fast. For example, it took just 25 iterations to achieve 10^{-7} accuracy in the components of q for the cluster of 2000 molecules of PTCDA, mentioned above.

Iterations (4) usually perform quite well. However, they are not guaranteed to converge and sometimes fail. For example, we found intermittent convergence problems for a pentacene cation in a layer on a metal substrate. Image charges in the metal induce strong charge redistribution along the pentacene axis with largest polarizability. On the other hand, the surrounding molecules in the layer have the opposite effect of drawing charge into the inside of the layer, closer to the center of the ion. As follows from the self-consistent solution, the second effect outperforms the first. This clearly leads to difficulties because the initial iterations tend to drive the system away from the convergence point, indicating also that a perturbative solution may be counterintuitive in this case.

Computational difficulties of this kind are rare. We now describe an alternative approach to solving polarization equations, which is formally stable and is guaranteed to converge, while it may not be as efficient as Eqs. (4).

B. Subspace methods for polarization problems

Let us return to the original Eq. (2). We can treat it as a general linear system

$$Aq = b, \quad (5)$$

with a symmetric matrix $A = G + V$ on the left-hand side. Solution of such a linear system is equivalent to minimizing the energy functional

$$E(q) = \frac{1}{2}(qAq) - (bq), \quad (6)$$

whose minimum exists when A is positive-definite.

We present a variationally-stable subspace approach to solving (5) based on the minimum principle (6). By rescaling the solution we can assume the right-hand side to be normalized, $(bb) = 1$. We shall be searching for the solution q in the Krylov subspace \mathcal{K} of the matrix A , generated by the vector b : $\mathcal{K} = \text{span}(b, Ab, A^2b, \dots, A^{m-1}b)$. At every step m we add a new vector to the subspace \mathcal{K} and construct the best vector q which minimizes (6) within \mathcal{K} . This guarantees that each step m yields a better solution, and thus the procedure converges.

We use the Hermitian Lanczos recursion [10,11] to build an orthonormal basis in \mathcal{K} : $q^{(1)} = b$,

$$q^{(m+1)} = \beta_{m+1}^{-1}(Aq^{(m)} - \alpha_m q^{(m)} - \beta_m q^{(m-1)}) \quad (7)$$

where α_m and β_m are chosen at each step m to orthogonalize $q^{(m+1)}$ with respect to both $q^{(m)}$ and $q^{(m-1)}$, ensuring that $(q^{(m)}|q^{(n)}) = \delta_{mn}$ for every m and n . Expressing $q = \sum_m c_m q^{(m)}$ and solving for the coefficients c_m that minimize $E(q)$ we find that they obey a linear system $\sum_n \tilde{A}_{mn} c_n = \tilde{b}_m$, where $\tilde{A}_{mn} = (q^{(m)}|Aq^{(n)})$ and $\tilde{b}_m = (q^{(m)}|b)$.

The algebraic properties of Lanczos recursion (7) yield readily all the components of \tilde{A} and \tilde{b} . The matrix \tilde{A} is symmetric tridiagonal with the diagonal elements $\tilde{A}_{mm} = \alpha_m$ and sub-diagonal elements $\tilde{A}_{m,m-1} = \beta_m$. Due to the special choice of $q^{(1)} = b$, all $\tilde{b}_m = 0$, except $\tilde{b}_1 = 1$ and $\tilde{b}_2 = \alpha_1$.

The method described above is variationally stable, since it is based on a minimum principle. Its drawback, however, is that it is generally slower than iterations (4). The reason is that Eqs. (4) follow from the dual form of Eqs. (3), which is based in turn on a physical insight of solving each molecule separately in the external field of other molecules. The subspace approach is not based on such an insight. In practice, it takes 200–300 iterations, rather than 25–35, to achieve convergence with this approach. Thus we use the subspace approach only when iterations fail.

C. Subspace method for non-positive definite cases

The subspace method of the above section being applied to Eq. (2) deals with the stiffness matrix G . It is preferable numerically to work with Π , rather than with its inverse. The reason is that whenever there is a small polarizability, e.g. in the direction normal to the plane of a π -conjugated molecule, it translates into a small eigenvalue of Π and, correspondingly, into a large eigenvalue of G . Numerically, it is much easier to handle near-zero than near-infinity.

In a more drastic situation, G may have negative eigenvalues, yet the polarization self-consistent equations (3)

continue to make sense. For example, we have introduced atomic polarizabilities $\tilde{\alpha}$ [6] as the difference $\alpha - \alpha^C$ between the best available molecular α and α^C based on semiempirical atomic charges. Usually α^C underestimates α by $\sim 10\%$. But the charge-induced polarizability occasionally exceeds α in some directions (see e.g. Table I), and the correction $\tilde{\alpha}$ has one or more negative eigenvalues. The self-consistent polarization equations (3) then give a saddle point of the energy functional, which formally has no minimum.

In order to use the subspace method to deal with Π rather than G , we rewrite Eqs. (3) in a matrix form in such a way that the matrix on the left-hand side is symmetric:

$$\begin{pmatrix} -V & 1 \\ 1 & \Pi \end{pmatrix} \begin{pmatrix} q \\ p \end{pmatrix} = \begin{pmatrix} p^{(0)} \\ 0 \end{pmatrix}. \quad (8)$$

This is again a linear system of type (5), but of twice the size. The matrix is, however, not positive-definite, and so the above method based on the minimization of (6) cannot be applied.

We present a modified subspace approach that is applicable to linear systems of type (5) with symmetric matrix A that is not necessarily positive definite. Instead of searching for the minimum of (6) we minimize the residual norm.

$$Z(q) = \frac{1}{2}(Aq - b|Aq - b), \quad (9)$$

which is also equal to half the norm of the gradient, $\partial E(q)/\partial q = Aq - b$. Again, expressing the solution as $q = \sum_m c_m q^{(m)}$, but solving now for c_m that minimize $Z(q)$ we find another linear system, $\sum_n \tilde{Z}_{mn} c_n = \tilde{w}_m$, where $\tilde{Z}_{mn} = (q^{(m)} A^2 q^{(n)})$ and $\tilde{w}_m = (q^{(m)} A b)$.

After some algebra, we find that the matrix \tilde{Z} is symmetric 5-diagonal with the following nonzero elements: $\tilde{Z}_{mm} = \alpha_m^2 + \beta_m^2 + \beta_{m-1}^2$, $\tilde{Z}_{m,m-1} = (\alpha_m + \alpha_{m-1})\beta_{m-1}$, and $\tilde{Z}_{m,m-2} = \beta_{m-1}\beta_{m-2}$, while the right-hand side has all components zero except $\tilde{w}_1 = \alpha_1$ and $\tilde{w}_2 = \beta_1$. The above expressions for the elements of \tilde{Z}_{mn} can be found by consequently multiplying Eq. (7) by itself with m replaced with $m-1$, $m-2$, etc. We notice by inspection that $\tilde{Z} = \tilde{A}^2$, except for the last row and column.

Throughout this section we have assumed that all vectors are projected onto the subspace \mathcal{Q} to preserve charge conservation relations. We did not discuss preconditioning techniques, such as rescaling the variables, which may improve convergence.

III. POLARIZATION IN PENTACENE CRYSTALS

A. Gas-phase properties

We performed calculations of the electronic structure of pentacene in gas phase using B3LYP hybrid density

functional theory with the extensive 6-311++G(d,p) basis set available in Gaussian 98 [12]. D2h symmetry was assumed and the geometry was separately optimized for the neutral molecule, cation, and anion. Unrestricted Hartree-Fock (UHF) was used for the ions. Limited spin contamination was observed as estimated by the maximum deviation of the total spin $\bar{S}^2 = 0.769$ before annihilation. Comparison of the energies of the ions in the neutral and ionic optimized geometries yields the relaxation energies $\lambda_+ = 46$ meV for the cation and $\lambda_- = 68$ meV for the anion, under the assumption of equal zero-point contributions for the neutral molecule and ions. λ_+ compares well with the value of 59 meV derived from experiment [13].

The vertical ionization potential is found to be $I = 6.229$ eV, which is significantly below the recently reported experimental value of 6.589 eV [13]. Other values of 6.64 eV [14] and 6.74 eV [15] were reported previously. The calculated value of I must be corrected by the difference in zero-point energies before the direct comparison can be made, but zero-point differences are probably less than 360 meV.

The experimental value for the electronic affinity is known with an error bar. Our calculated B3LYP value $A = 1.475$ eV is 105 meV above the recommended average 1.37 eV [16] of experimental data. Thus, B3LYP values lead to the gas-phase pentacene charge gap $I - A = 4.754$ eV (without zero-point correction) vs. 5.22 eV derived from experiment.

B. Polarization energies

Following the procedure in [6] we first calculate atom-atom polarizabilities Π_{ij} for individual pentacene molecules using the semiempirical INDO/S Hamiltonian [17]. Experimental geometries from the crystal structure data [18] were used. Positions of hydrogen atoms, not known experimentally, were AM1-optimized using Gaussian 98 with the heavy atoms fixed.

Due to the inequivalence in crystal field for the two molecules in the unit cell, their geometries are slightly different. There are two atom-atom polarizability tensors Π_{ij} with i, j ranging over 36 atoms of a pentacene,

$$\Pi_{ij} = -\frac{\partial \rho_i}{\partial \phi_j} = -\frac{\partial^2 E}{\partial \phi_i \partial \phi_j} \quad (10)$$

E is the INDO/S ground-state energy, $\phi_i = \phi(\mathbf{r}_i)$ is the crystal potential at atom i and ρ_j are Löwdin atomic charges. Charge redistribution is then described explicitly as

$$\rho_i = \rho_i^{(0)} - \sum_j \Pi_{ij} \phi_j \quad (11a)$$

$$\boldsymbol{\mu}_i = \tilde{\alpha}_i \mathbf{F}_i, \quad (11b)$$

[cf. Eqs (3)], where $\rho_i^{(0)}$ are gas-phase charges, μ_i are induced atomic dipoles and $\mathbf{F}_i = -\nabla\phi(\mathbf{r}_i)$ are electric fields. $\tilde{\alpha} = \alpha - \alpha^C$ is a correction [6] that accounts for the difference in *ab-initio* molecular polarizability and the “charges-only” part α^C associated with Π_{ij} :

$$\alpha_{\alpha\beta}^C = \sum_{ij} \Pi_{ij} r_i^\alpha r_j^\beta. \quad (12)$$

We computed α for the two geometries using B3LYP density functional with 6-311++G(d,p) basis set of Gaussian 98.

Principal values of α and “charges-only” α^C are compared in Table I. Charge redistribution accounts quite well for the in-plane components α_{LL} and α_{MM} of the neutral molecule. The polarizability α_{NN} , normal to the molecular plane, is completely “atomic,” as expected, and cannot be described by charge redistribution [9,6]. Values that are not exactly zero are due to non-planar molecules in the crystal. The INDO/S results for ions are far too large; we return to this point in the Discussion.

Table I. Molecular polarizability of pentacene along principal axes (L = long, M = medium, N = normal)

Molecule	α_{NN} (\AA^3)	α_{MM} (\AA^3)	α_{LL} (\AA^3)
B3LYP/6-311++G**			
Neutral(1)	17.77	37.66	91.43
Neutral(2)	18.02	38.02	99.48
Anion(1)	19.87	40.16	135.47
Anion(2)	20.20	40.81	131.88
Cation(1)	16.31	35.91	130.87
Cation(2)	16.54	36.54	124.14
α^C, Eq. (12)			
Neutral(1)	0.06	39.26	87.41
Neutral(2)	0.05	39.61	95.83
Anion(1)	0.06	35.26	194.35
Anion(2)	0.05	39.98	231.24
Cation(1)	0.06	36.03	368.28
Cation(2)	0.05	40.55	282.52

The difference between the B3LYP and α^C in Table I is distributed over the atoms with the weight proportional to the atomic valence charge [6]. Since charge redistribution overestimates the in-plane molecular polarizability in pentacene, the atomic correction tensor $\tilde{\alpha} = \alpha - \alpha^C$ is not positive definite. It is still small, however, for neutral molecules, and the self-consistent solution is well defined, even though it does not correspond strictly to the minimum of the total energy (cf. discussion in II.C).

C. Properties of the neutral lattice

Both pentacene [18] and anthracene [19] illustrate herring-bone packing with two molecules per unit cell, but their Bravais lattices are different. Pentacene is triclinic [18]. The two molecules are inequivalent and subject to different crystal-field environments. The polarization energy of a cation or anion consequently depends on which molecular site is charged. Since crystalline electric fields are perturbations, we expect comparable polarization energies that differ at most by ~ 100 meV. Such differences have already been computed [20] in pentacene crystals using the submolecular method [7,21] in which the gas-phase molecular polarizability α is placed as $\alpha/5$ at the ring centers.

Solving self-consistent polarization equations for the neutral lattice of pentacene, we find that polarization contribution to sublimation energy is negligible (1.23 meV per molecule), as in anthracene, since the gas-phase charges are small due to an approximate electron-hole symmetry of the valence shell. We find the dielectric tensor of pentacene to be highly anisotropic, with principal values $\kappa_1 = 5.336$, $\kappa_2 = 3.211$, and $\kappa_3 = 2.413$. For reference purposes, the directional cosines of the principal axes are $\mathbf{n}_1 = (-0.296, -0.314, 0.902)$, $\mathbf{n}_2 = (-0.021, 0.946, 0.322)$, and $\mathbf{n}_3 = (0.955, -0.076, 0.286)$, respectively, in the Cartesian coordinate system with the pentacene lattice vectors (in \AA) $\mathbf{a} = (7.900, 0, 0)$, $\mathbf{b} = (0.444, 6.044, 0)$, and $\mathbf{c} = (-6.153, -2.858, 14.502)$. The direction of \mathbf{n}_1 coincides with the direction of long axes of pentacene molecules to the accuracy to which the latter can be defined ($\sim 5^\circ$).

The calculated principal axes and values of κ for anthracene crystals agree with experiment [9]. Measurements of refractive indices or optical dielectric constants are challenging in anisotropic molecular crystals [22]. We are not aware of such data for pentacene crystals. Dielectric data will be necessary for organic devices with improved performance.

D. Charge carriers in the bulk

We compute the polarization energy of charge carriers following [6], by placing an ion in the infinite neutral lattice and considering an imaginary sphere of M molecules surrounding it. We allow only the molecules whose centers fall into the sphere to relax their charge distributions from the self-consistent values for the neutral lattice and monitor convergence as M is increased. We use the same molecular geometry for the ion. The small (~ 100 meV) relaxation energies of large aromatic molecules make the same geometry both an excellent and convenient approximation. Atom-atom polarizabilities Π_{ij} for the ion are computed using unrestricted Hartree-Fock (UHF) INDO/S.

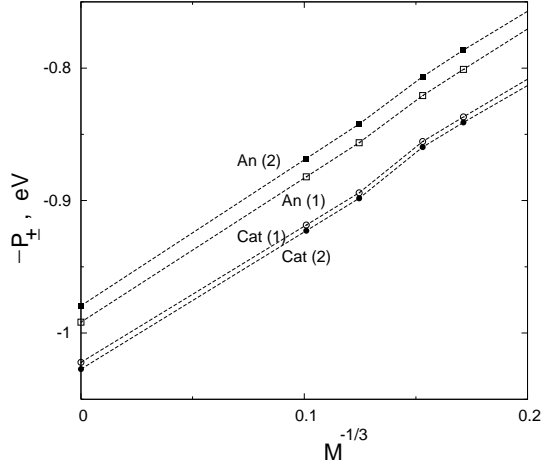


Fig. 2 Convergence of P_{\pm} with increasing cluster size M .

Figure 2 shows linear convergence of polarization energy with $M^{-1/3}$, which is proportional to the inverse radius of the sphere. The polarization energy extrapolates as $\propto M^{-1/3}$, because the missing part at large finite M can be thought of as polarization of an infinite homogeneous dielectric with a spherical cavity of radius $R \propto M^{-1/3}$, $-(1 - \kappa_{\text{eff}}^{-1})e^2/R$ [6]. Extrapolation to infinite radius gives the polarization energy in the bulk, $P = P_+ + P_- = 2.014$ eV and 2.007 eV for the ion occupying positions 1 and 2 in the unit cell, respectively. The “charges only” values of $P = P_+ + P_-$ are $\sim 10\%$ less, as also found in other organic crystals. Since κ_{eff} for an anisotropic dielectric medium is known [23], the slope in Fig. 2 at large M is directly related to the κ_{α} found above, and the slopes agree within a few percent. We note that κ_{eff}^{-1} implies identical slopes at large M for the anion and cation in either position, as found separately in Fig. 2.

Using B3LYP values for I and A in the gas phase, we calculate the transport gap of the pentacene crystal $E_t = I - A - P = 2.740$ eV in the limit of zero overlap. This correlates quite well with the reported band gap of 2.85 eV, obtained from careful fit of electroabsorption spectra [20]. $E_t = 2.78$ eV was reported in [24] also based on electroabsorption spectra of charge-transfer (CT) states. The experimental value for the charge gap, $I - A = 5.22$ eV, used in this context results in $E_t = 3.21$ eV, which is too high.

E. Ion pairs and CT states

We next report polarization energies P_{pair} of CT states with an ion at the origin and the counter ion at a nearby site. We place the ion pair within an imaginary sphere in a neutral lattice and calculate the effective interaction V_{eff} , which is the difference of the total polarization energy and the energy of a pair of well-separated charges,

$V_{\text{eff}} = (P_{\text{pair}} - P_+ - P_-)$. $-V_{\text{eff}}$ is the binding energy of CT states in the limit of no overlap and is closely related to the binding energies of Frenkel excitons, when the final state is a molecular excitation.

Fig. 3 shows convergence with the size of the sphere. Since the total ion charge within the sphere is zero, the leading term $\propto M^{-1/3}$ vanishes. The polarization energy of a dipole in a dielectric medium converges much faster as $\propto M^{-1}$. Extrapolating to infinite M , we obtain the lowest CT states at -0.719 and -0.679 eV for the nearest-neighbors (center-to-center distance 4.799 Å) and -0.685 and -0.675 eV for next-nearest neighbors (5.151 Å), as listed in Table II. These results compare reasonably with submolecular calculations [20] of -0.777 and -0.698 eV, respectively, with $\alpha/5$ at ring centers. Submolecular results do not distinguish between anions and cations and also depend on the precise partitioning of α , which is left open.

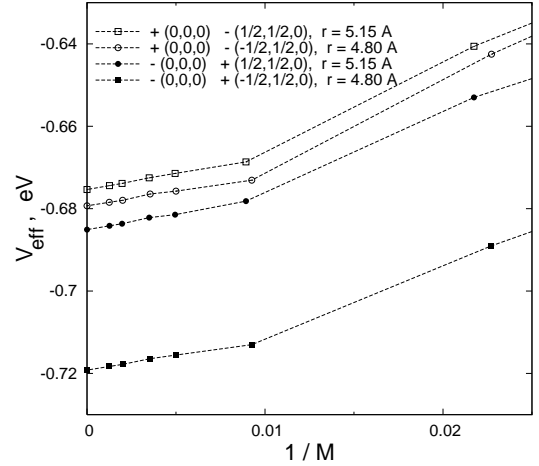


Fig. 3 Convergence of the effective electron-hole interaction energy with cluster size M .

Table II. Effective interaction energies $V_{\text{eff}}(\mathbf{r})$, in eV, of cation-anion pairs. The submolecular data is from [20]. Center-to-center distances r are also listed for reference.

Anion	Cation	r , Å	$V_{\text{eff}}(\mathbf{r})$	$V_{\text{eff}}^{\text{submol}}(\mathbf{r})$
(0, 0, 0)	$(-\frac{1}{2}, \frac{1}{2}, 0)$	4.7990	-0.719	-0.756
$(-\frac{1}{2}, \frac{1}{2}, 0)$	(0, 0, 0)	4.7990	-0.679	-0.756
(0, 0, 0)	$(\frac{1}{2}, \frac{1}{2}, 0)$	5.1514	-0.685	-0.698
$(\frac{1}{2}, \frac{1}{2}, 0)$	(0, 0, 0)	5.1514	-0.675	-0.698

It is interesting that the mutual orientation of the cation and ion together with variations in their electrostatic response are enough to reverse the order of states, such that the pair with larger center-to-center distance has greater binding energy (lines 2 and 3 in Table II). This is an effect very similar in nature to the one suggested by Mazur and Petelenz [25].

IV. POLARIZATION IN PENTACENE FILMS

A. Inert metal-organic interfaces

We now address polarization energy in thin pentacene films deposited on metal surface (Fig. 1). We use an approach similar to the one sketched recently for thin films of PTCDA [5], which we present in greater detail. We assume an ideal metal-organic interface without chemical interactions. Organic molecules are physisorbed and in van der Waals (vdW) contact with the metal. We model the metal as an equipotential surface parallel to the organic layer. The potential at the metal is assumed to be $\phi = 0$, as the actual value drops out from the combined polarization energy for the electron and hole, $P = P_+ + P_-$, even though we perform separate calculations for P_+ and P_- . In fact, any additive constant in the potential cancels out for any neutral entity with an arbitrary but equal numbers of positive and negative charges.

For the organic film we use the bulk crystal geometry, assuming a parallel slab of the crystal cut along molecular layers and placed parallel to the metal surface. The only parameter in the model that allows limited adjustment is the actual distance of the equipotential plane from the slab. We choose it such that the equipotential surface is at the vdW contact distance of 2.80 Å between the closest hydrogen and gold atoms. The molecular arrangement depicted in Fig. 1 is in fact drawn to scale.

As in [5] the equipotential metallic surface is treated by means of the image charges. For each atomic partial charge and induced dipole we assign and place an opposite charge and dipole in mirror positions when computing potentials and potential gradients. The charges and dipoles within a molecule do not contribute to the potentials and potential gradients that act on that molecule. However, the images of these charges and dipoles do contribute. For example, a single ion exhibits no polarization energy in gas phase, while it acquires polarization energy when placed near the metal surface.

As in bulk calculations, we solve the polarization problem for slabs in two steps. We first consider a neutral film of N molecular layers with no ions and with translational symmetry in two dimensions. We solve the self-consistent equations and find ground-state charges $\bar{\rho}_i^{kj}$ and dipoles $\bar{\mu}_i^{kj}$, which are different for each molecular layer $k = 1, \dots, N$ and for each type $j = 1, 2$ of molecule in the unit cell. While the slab is infinite in two dimensions, the number of variables is finite due to translational symmetry.

We then replace one molecule in the surface molecular layer by an ion and solve for the difference $\delta\rho_i^a = \rho_i^a - \bar{\rho}_i^{kj}$ and $\delta\mu_i^a = \mu_i^a - \bar{\mu}_i^{kj}$ for every molecule a in the slab. Since the slab is infinite, we define clusters whose shapes are pillboxes with variable radius R parallel to the metal

and fixed thickness to include N molecular layers and their images. We then relax the charge distribution of all M molecules whose centers are in the pillbox. We assume $\delta\rho_i^a = \delta\mu_i^a = 0$ for the molecules a outside the pillbox, which means that their charge distributions are not relaxed. They contain, however, partial charges and dipoles $\bar{\rho}_i^{kj}$ and $\bar{\mu}_i^{kj}$, which contribute to the total polarization energy of the film.

B. Surface and interface polarization

The polarization energy for the ion appears, as in the bulk, as a finite difference of two infinite energies: for the infinite slab with and without the ion. The expression for the energy that takes care of this cancellation is the same as Eq. (27) in [6], but with the potentials and potential gradients containing contributions from image charges and dipoles. We perform calculations for finite pillbox clusters of increasing M , and extrapolate to $M \rightarrow \infty$.

Fig. 4 shows the convergence of polarization energies for cations (upper panel) and anions (lower panel), as well as the extrapolated values for pentacene films one to ten molecular layers thick. Two lines for each film thickness correspond to two types of molecules in the unit cell. Convergence with increasing pillbox radius R is shown as $1/M_l$, where $M_l = M/N$ is the average number of pentacenes per layer. The computational effort increases with N . The largest $N = 10$ clusters in Fig. 3 contain $M = 2806$ molecules, each containing 36 atoms, and their images.

The combined extrapolated values $P^S = P_+^S + P_-^S$ are also listed in Table III and plotted vs. $1/N$ in Fig. 5. The monolayer ($N = 1$) and bulk values are almost the same. Image charges and dipoles at vdW separation are sufficiently more polarizable to compensate for a vacuum on the other side. $P^S(N)$ decreases with increasing N as less polarizable organic layers are introduced between the surface and the metal. In the limit of a thick film, or a free pentacene *ab* surface, we estimate $P^S - P \sim -0.23$ eV.

Table III. Variation in polarization energy at the surface (P^S) and at the metal/organic interface (P^M) in an N -layer thick pentacene film on a metallic substrate. The values are reported for anion at position (1) and cation at position (2) in the unit cell, which correspond to the lowest energy state.

Layers, N	$(P^S - P)$, meV	$(P^M - P)$, meV
1	6	6
2	-40	113
3	-71	125
5	-108	129
10	-166	130
thick film	-227	130

In Table III the interface values $P^M = P_+^M + P_-^M$ refer to the polarization energy of an ion next to the metal in a film of N molecular layers. The biggest increase of 100 meV at $N = 2$ comes from the first pentacene overlayer. Additional layers produce small changes and the interface value in a thick films is $P^M - P = 0.13$ eV. The hole and electron components of P^M are relevant for matching transport levels to Fermi energies for facile injection of carriers. Such optimization for organic devices is largely empirical at present, often without *any* consideration of polarization. The variation of $P^S(N)$ or $P^M(N)$ with film thickness is less in pentacene than in PTCDA [5]. Pentacene layers are several times thicker, with the long axis normal to the metal, and a single layer already provides an effective polarization environment for the charge.

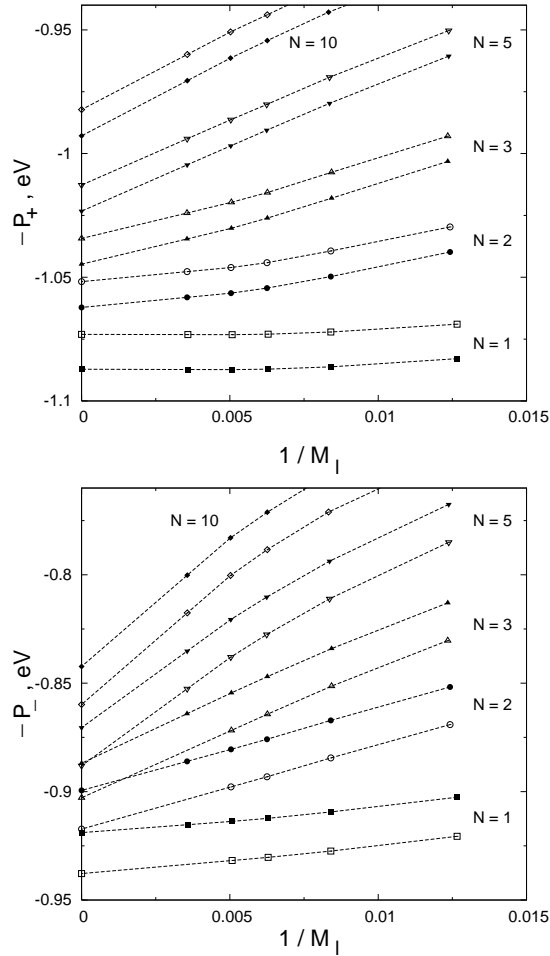


Fig. 4 Convergence of polarization energies of a cation (upper panel) and anion (lower panel) in the outermost surface layer of pentacene film on gold vs. the average number $M_l = M/N$ of molecules in each molecular layer (M molecules in N layers in the pillbox). Open and solid symbols correspond to the molecules of type (1) and (2) respectively.

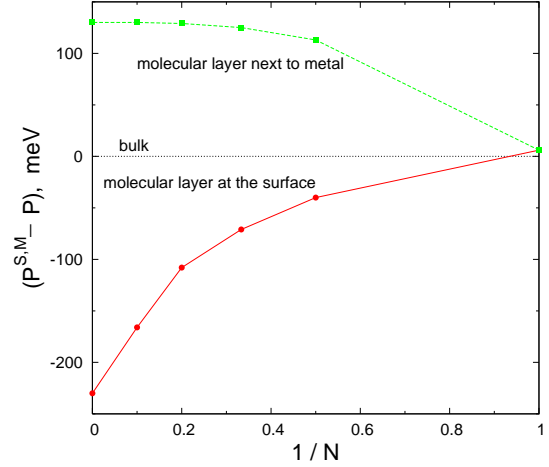


Fig. 5 Variation in polarization energy at the surface ($P^S(N) - P$) and at the metal/organic interface ($P^M(N) - P$) for an N -layer thick pentacene film on a metal substrate.

C. Molecular potential

We have already noted the competition between image charges and induced dipoles in films of molecules with large polarizability normal to the surface. The self-consistent potential $\phi^a(\mathbf{r})$ at molecule a is due to the polarized densities $\rho^b(\mathbf{r})$ of all other molecules and their images. A single pentacene cation in the surface layer induces an image anion in the metal. Since the interaction is attractive, the cation's $\phi^{cat}(\mathbf{r})$ increase monotonically with the distance from the surface. Similarly, the $\phi^{an}(\mathbf{r})$ of a single anion on the surface decrease monotonically with distance from the surface.

The situation in films is quite different due to the surrounding neutral molecules. Since the large pentacene polarizability is normal to the surface, the induced moments due to the image anion are parallel. The repulsion of parallel dipoles and image dipoles is relieved by redistributing charge towards the middle of the molecular layer. Now the $\phi^{cat}(\mathbf{r})$ has a minimum at atoms near the center, while the $\phi^{an}(\mathbf{r})$ has a maximum near the center. The actual $\phi^{ion}(\mathbf{r})$ in the limit of zero overlap is the solutions of the self-consistent equations.

Figure 6 shows the self-consistent potential $\phi^{cat}(\mathbf{r})$ for \mathbf{r} along the axis of a cation in a pentacene monolayer on metal. The gradients yield electric fields $\pm 10^7$ V/cm that reverse over a single molecule, directly confirming that fields are strong and non-uniform. The variation of $\phi^{cat}(\mathbf{r})$ with \mathbf{r} shows the importance of repulsion between induced dipoles. Image charges account for more negative $\phi^{cat}(\mathbf{r})$ close to metal. Similar variations of self-consistent potentials are found at ions (1) and at neighboring neutral molecules. The strong shielding of a single layer of pentacene follows from the weak dependence on

N . Similar curves (not shown) for $N = 2, 3$, and 5 are essentially parallel to the $N = 1$ curve in Fig. 6, but displaced to less negative (positive) potential for cations (anions).

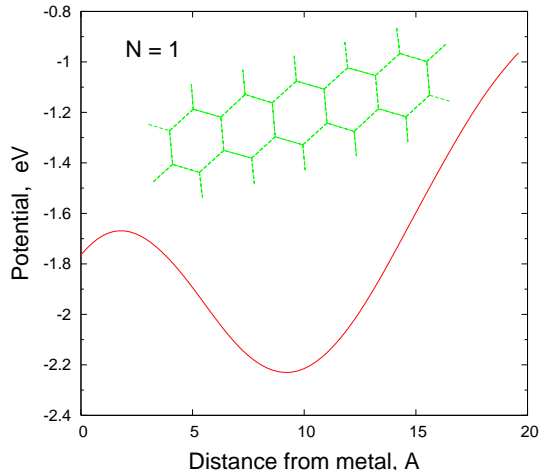


Fig. 6 Self-consistent potential for a cation created by the polarization field of neutral molecules in the lattice and the image charge distribution in the metal. Data shown for a cation in a monolayer on metal substrate, placed in the position (2) in the unit cell. The sketch of the molecule shows actual position with respect to the metal.

V. DISCUSSION

The bulk polarization energy can be estimated simply in terms of molecular size, $P_{\pm} = (e^2/2R)(1 - 1/\kappa)$, for a sphere of radius R in an isotropic dielectric medium with $\kappa \sim 3$ for organic molecular crystals. Such rough values rationalize much data but preclude accurate positioning of transport or CT states. The effective pentacene radius is 14% greater than that of anthracene, while the polarization energy decreases by only 9%. On the other hand, the radii of pentacene and PTCDA molecules are the same within 3%, but the polarization energy differs by 10%. The greatest contrast to PTCDA films [5], is that the polarization energy P^S is within 10% of the bulk value in pentacene, compared to $P^S/P = 0.77$ in PTCDA.

Direct relations between gas-phase and crystalline energies have long been sought using molecular exciton theory [7,26]. Accurate evaluation of electronic polarization permits sharper comparisons. There is considerable scatter in reported values for both the gas and solid, as noted in Sections III(A) and III(D) for the ionization potential and electron affinity of pentacene. The transport gap is $I - A - P$ in the limit of zero intermolecular overlap. The experimental values for the pentacene transport gap range from 2.85 eV [20] to 2.4 eV suggested in [27], to 2.2 eV used in [28]. This scatter was not “important”

when polarization energies had to be estimated in the bulk and were not available at all at surfaces. With the ability to calculate polarization energies, it becomes possible to analyze and connect various sources of experimental data on such quantities as optical and transport gaps, CT binding energies, and work functions.

All molecular calculations, except for the gas-phase properties, were performed using experimental geometries from the crystal structure data [18]. Slight variations in the geometry of the two molecules in the unit cell were consequently taken into account. While the variations in electronic energies are small (tens of meV), which is consistent with the adopted approximation, we believe that crystalline geometries are preferable to gas-phase geometries when vertical electronic transitions are considered in the condensed phase.

We note that INDO/S greatly overestimates the in-plane polarizabilities of ions in Table I. The huge difference of α^C between cations 1 and 2 is clearly unphysical in view of small distortions in the crystal, and it rationalizes why convergence was particularly difficult for cation 1. The UHF INDO/S approach fails for ions. Radical ions of large conjugated molecules are expected to be more polarizable than the neutral molecules, in line with the B3LYP entries in Table I. While the idea is that $\tilde{\alpha}$ constitutes a small correction, and it is not so for ions, we expect this to have a negligible impact on the results. The reason is that the largest part of the polarization energy comes not from the ion itself but from the polarization of many neutral molecules surrounding it. Moreover, the molecular α is kept no matter how it is partitioned between charge redistribution (α^C) and induced dipoles. In the future we may choose to use Π_{ij} of the neutral molecule for the ions, and to absorb the polarizability difference in $\tilde{\alpha}$. This requires separate B3LYP calculation of α for the ions, as done here, but not in [6].

Small atomic charges in acenes are related to approximate electron-hole symmetry. The crystal potential $\phi_i = \phi(\mathbf{r}_i)$ at atom i due to INDO/S charges is consequently small, as shown by ~ 1 meV per molecule contributions to the sublimation energy. Since the potential due to the B3LYP or any other gas-phase charge distribution can readily be computed at the positions of other atoms in the crystal, we can obtain first-order corrections to polarization energies in general [29] by combining the best available gas-phase potential with self-consistent charges and dipoles based in INDO/S calculations. The quadrupole moments of acenes lead to opposite shifts of P_+ and P_- , as discussed previously for submolecules [7,21]. Since such corrections cancel in $P = P_+ + P_-$ in anthracene [6], we expect them to be small in pentacene. They are not negligible in PTCDA or conjugated molecules that contain heteroatoms and hence partial charges.

Our values for the the transport gap are likely an overestimate, due to the bandwidth effects for electrons and

holes, and the correction can be introduced as $E_t = I - A - P - W$. The bandwidth W in molecular crystals at room temperature is thought to be of the order of few tens of meV or less, which justifies our zero-overlap approximation. At lower temperatures, however, the bandwidths may be large in certain directions. It has been suggested that the bandwidth in pentacene (at zero temperature) may be anomalously large and reach 500 meV [30]. If we estimate $W \sim 0.5$ eV, we get $E_t = 2.71$ eV with the experimental charge gap, while the calculated charge gap leads to the value 2.35 eV, which is too small.

When bandwidths are comparable to polarization energies, the zero-overlap approximation cannot be justified, and we face a challenging problem of combining the “localized” treatment of polarization effects with the “de-localized” language of band theory. The self-consistent polarization approach can provide a proper “zero-order” approximation for the attempts to treat bandwidth effects as perturbation.

We note that our self-consistent approach has the ability to distinguish between the electronic polarization of cations and anions, since the quantum-mechanical structure of molecular response is used to obtain the redistribution of charge. We can also estimate variations of polarization caused by slight changes in molecular geometry between crystal and gas-phase, and especially between inequivalent molecules in the unit cell. These variations appear to be of the order of 20–40 meV, which is on the threshold of the accuracy, but such variations are probably correct on the order of magnitude, and may be important in the analysis of experimental data.

In summary, we have applied the recently developed self-consistent approach based on evaluating charge redistribution in organic molecules to the problem of electronic polarization in pentacene molecular crystals. The power of the approach comes from the combination of semiempirical treatment of charge distribution by means of atom-atom polarizability tensors with accurate *ab initio* gas-phase calculations of molecular polarizabilities. As a result, we are now able to calculate polarization energies with accuracy on the order of 0.1 eV or better.

ACKNOWLEDGMENTS

It is a pleasure to thank A. Kahn and R.A. Pascal, Jr. for stimulating discussions. We gratefully acknowledge support for work at Rutgers through the Office of Naval Research, grant No. NO00014-01-1-1061, and at Princeton through the MRSEC program under DMR-9400632.

-
- [1] G. Horowitz, Adv. Mat. **10**, 365 (1998).
- [2] Y.Y. Lin, A. Dodabalapur, R. Sarpeshkar, Z. Bao, W. Li, K. Baldwin, W.R. Raju, and H.E. Katz, Appl. Phys. Lett. **74**, 2714 (1999).
- [3] S.R. Forrest, Chem. Rev. **97**, 1793 (1997).
- [4] I.G. Hill, A. Kahn, Z.G. Soos, and R.A. Pascal, Jr., Chem. Phys. Lett. **327**, 181 (2000).
- [5] E.V. Tsiper, Z.G. Soos, W. Gao, and A. Kahn, Chem. Phys. Lett. **360**, 47 (2002).
- [6] E.V. Tsiper and Z.G. Soos, Phys. Rev. **B64**, 195124 (2001).
- [7] E.A. Silinsh and V. Capek, *Organic Molecular Crystals: Interaction, Localization and Transport Phenomena* (Am. Inst. Phys., New York, 1994).
- [8] I.V. Brovchenko, Chem. Phys. Lett. **278**, 355 (1997).
- [9] Z.G. Soos, E.V. Tsiper, and R.A. Pascal Jr., Chem. Phys. Lett. **342**, 652 (2001).
- [10] C. Lanczos, J. Res. Nat. Bur. Standards **45**, 255 (1950).
- [11] B.N. Parlett, *The symmetric eigenvalue problem*, (Prentice Hall, Inc, London, 1980).
- [12] M.J. Frisch et al., GAUSSIAN 98 (Gaussian Inc, Pittsburgh, 1995).
- [13] N.E. Gruhn, D.A. de Silva Filho, T.G. Bill, M. Malagoli, V. Coropceanu, A. Kahn, and J.-L. Bredas, JACS **124**, 7918 (2001).
- [14] P.A. Clark, F. Brogli, and E. Heilbronner, Helv. Chim. Acta **55**, 1415 (1972).
- [15] R. Boschi, J.N. Murrell, and W. Schmidt, Discuss. Faraday Soc. **54** (1972); R. Boschi, E. Clar, and W. Schmidt, J. Chem. Phys. **60**, 4406 (1974).
- [16] N. Sato, H. Inokuchi, and E.A. Silinsh, Chem. Phys. **115**, 269 (1987).
- [17] M.C. Zerner, G.H. Loew, R.F. Kirchner, and U.T. Mueller-Westerhoff, J. Am. Chem. Soc., **102**, 589 (1980).
- [18] R.B. Campbell, J.M. Robertson, and J. Trotter, Acta Cryst. **15**, 289 (1962).
- [19] C.P. Brock and J.D. Dunitz, Acta Cryst. **B 46**, 795 (1990).
- [20] P. Petelenz, M. Slawik, K. Yokoi, and M.Z. Zgierski, J. Chem. Phys. **105**, 4427 (1996).
- [21] J.W. Rohleder and R.W. Munn, *Magnetism and Optics of Molecular Crystals* (Wiley, New York, 1992) and references therein.
- [22] N. Karl, H. Rochrbacher, and D. Siebert, Phys. Status Solidi **A4**, 105 (1971).
- [23] P.J. Bounds and R.W. Munn, Chem. Phys. **44**, 103 (1979).
- [24] P.J. Bounds, W. Siebrand, I. Eisenstein, R.W. Munn, and P. Petelenz, Chem. Phys. **95**, 197 (1985).
- [25] G. Mazur and P. Petelenz, Chem. Phys. Lett. **324**, 161 (2000).
- [26] M. Pope and C.E. Swenberg, *Electronic Processes in Organic Crystals* (Clarendon, Oxford, 1982).
- [27] L. Sebastian, G. Weiser, and H. Bassler, Chem. Phys. **61**, 125 (1981).
- [28] N. Koch, J. Ghijsen, R.L. Johnson, J. Schwartz, J.-J. Pireaux, and A. Kahn, J. Phys. Chem. B **106**, 4192 (2002).
- [29] J.M. Sin, E.V. Tsiper, and Z.G. Soos, Europhys. Letters **60**, 743 (2002).
- [30] J. Cornil, J.Ph. Calbert, and J.L. Bredas, JACS **123**, 1250 (2001).